



# Quantitative attribution of vertical motions responsible for the early spring drought conditions over southeastern China

Zejiang Yin<sup>1,2</sup> · Song Yang<sup>1,2</sup> · Wei Wei<sup>1,2</sup>

Received: 8 October 2022 / Accepted: 7 February 2023 / Published online: 18 February 2023  
© The Author(s) 2023

## Abstract

The interannual variability and long-term trend of the drought conditions over southeastern China during early spring (from February to April) are investigated by analyzing the standardized precipitation evapotranspiration index in 1979–2020. Results from an attribution analysis show that precipitation deficiency and atmospheric water demand contributes about 96.5 and 6.7% to the drought conditions on interannual time scale, and about 72.8 and 22.3% to the long-term trend, respectively. The precipitation deficiency is primarily contributed by moisture divergence via the descending anomalies throughout the troposphere over southeastern China. A further diagnosis with the omega equation reveals that the descending anomalies are dominated by the strong negative zonal vorticity advection in the upper troposphere and the enhanced meridional cold advection throughout the troposphere. They are controlled by a barotropic anomalous anticyclone over the eastern Tibetan Plateau and an anomalous cyclone over the western North Pacific. Non-negligibly, the contribution of potential evapotranspiration to the drying trend in early spring over southeastern China is about four times larger than that to the interannual variability. Given that potential evapotranspiration may increase in a warming climate, it may be critical for the change in drought conditions in future. This study serves as a basis for fully understanding the severity of recent droughts and for model simulation of the drought conditions over southeastern China.

**Keywords** Southeastern China · Early spring · Drought · Interannual variability · Long-term trend · Dynamical diagnosis

## 1 Introduction

Droughts are one of the most damaging natural disasters (Keyantash and Dracup 2002). They destructively results in severer water shortage and crop yield reduction or failure (Montaseri and Amirataee 2017). Generally, droughts can be classified into meteorological droughts, agricultural droughts, hydrological droughts, and economical–social droughts (Mishra and Singh 2010). The latter three types of droughts are usually originated from meteorological droughts (Gu et al. 2020; Ding et al. 2021). Associated with global warming, more frequent and severe meteorological

drought events have occurred over arid and relatively humid regions such as Africa, East and South Asia, southern Europe, eastern Australia, and many places of the Americas (Dai and Zhao 2017; Spinoni et al. 2020).

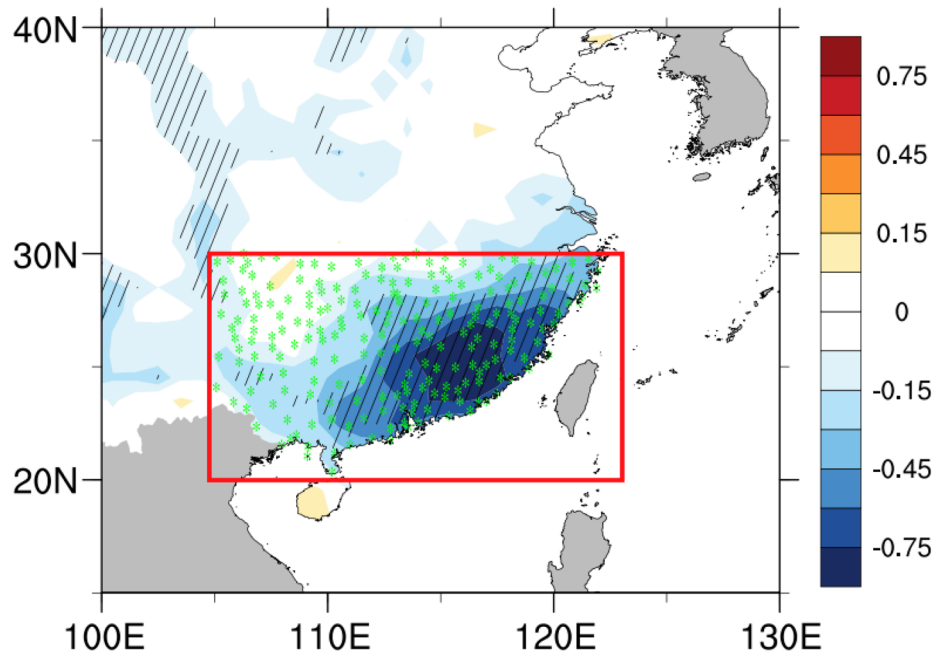
Southeastern China (SE China), one of the most populated regions and an important grain base, is vulnerable to drought risk (Zhang et al. 2019; Zhou et al. 2020). During the past decades, drought hazards have notably increased in SE China, causing increased agricultural and economic losses (Zhang et al. 2019). Spinoni et al. (2020) suggested that SE China was one of the meteorological drought hot spots with more frequent, severe, and extreme droughts in the future. Observations show that SE China has experienced a drying trend in spring (Fig. 1; Li et al. 2017). During the transitional period from dry to wet, the surface water balance between precipitation and potential evapotranspiration (PET) changes from deficiency (from September to February) to surplus (from Mar to August) in early spring (Fig. 1b). The drought conditions over SE China generally peak in early spring when following a dry winter (Xie et al. 2007; Sun and Yang 2012). Thus, spring droughts in SE

✉ Wei Wei  
weiwei48@mail.sysu.edu.cn

<sup>1</sup> School of Atmospheric Sciences, Sun Yat-sen University; and Southern Marine Science and Engineering Guangdong Laboratory (Zhuhai), Zhuhai 519082, China

<sup>2</sup> Guangdong Province Key Laboratory for Climate Change and Natural Disaster Studies, Sun Yat-sen University, Zhuhai, China

## (a) Trends in P-PET



## (b) Clim. &amp; Trends in P-PET

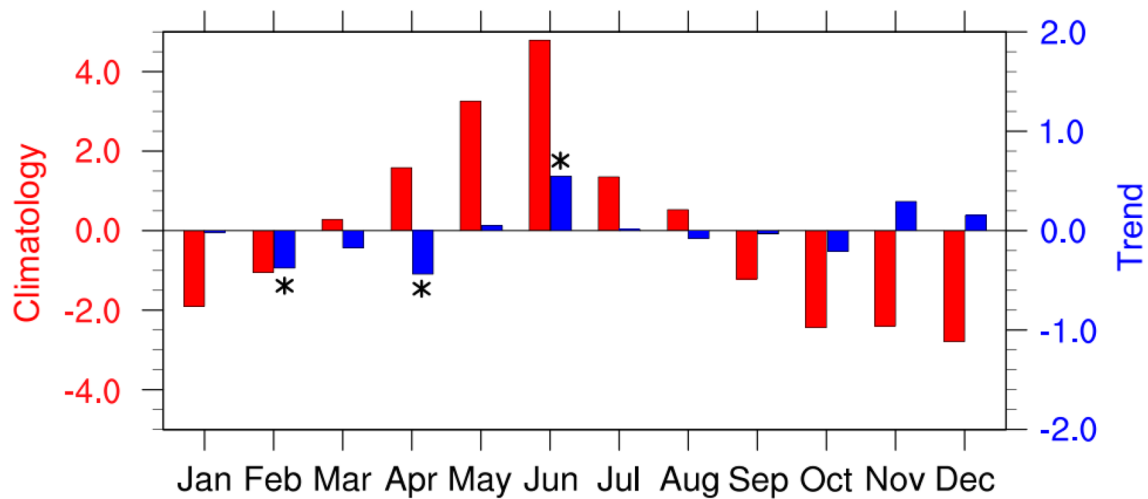


**Fig. 1** **a** Linear trends of precipitation minus PET in FMA (unit:  $\text{mm day}^{-1} \text{ decade}^{-1}$ ). Significant values exceeding the 0.1 and 0.05 significance levels are marked by gray and black dots, respectively; **b** the annual cycle of monthly anomalies (left vertical axis; red bars; unit:  $\text{mm day}^{-1}$ ) and linear trends (right vertical axis; blue bars; unit:  $\text{mm day}^{-1} \text{ decade}^{-1}$ ) of precipitation minus PET averaged over SE China. The significant values of trends exceeding the 0.05 significance level are indicated by hatched lines. The positions of stations in SE China are represented by green asterisks

$\text{day}^{-1} \text{ decade}^{-1}$ ) of precipitation minus PET averaged over SE China. The significant values of trends exceeding the 0.05 significance level are indicated by hatched lines. The positions of stations in SE China are represented by green asterisks

China are more intense and last longer, and substantially more destructive than other seasons (Oh et al. 2014; Park et al. 2020). In 2011, a long-lasting severe drought from the peak winter to late spring in southern China destroyed more than 98.9 million hectares of crops and leaved more than 4.9 million people lack of potable water (Sun and Yang 2012). Considering the enormous adverse effects of early spring

droughts in SE China, it is necessary to further investigate the variations of early spring drought conditions and the responsible mechanisms.

Meteorological droughts are related to surface water balance. In relatively humid regions, precipitation deficiency plays a crucial role in the development of droughts (Xin et al. 2006; Chen and Sun 2015), and the fluctuation in

precipitation is adequate to represent the temporal variability of droughts in wet season (Xu et al. 2015; Suroso et al. 2021). However, in relatively dry season, atmospheric water demand (e.g., PET) also plays an important role since its variability is comparable to that of precipitation (Song et al. 2014; Sun et al. 2018). Thus, it deserves further investigation that whether atmospheric water demand plays an important role in the drought conditions in the relative dry season over SE China. Especially in the warming climate, the significantly increasing temperature and atmospheric water demand are critical to the change in drought conditions (Dai et al. 2004; Milly and Dunne 2016). Li et al. (2020) suggested that the increasing drought severity, area, and frequency in China during the recent decades were mainly due to the increasing PET. Thus, it is necessary to quantify the contributions of atmospheric water supply (e.g., precipitation) and demand to the variations of early spring drought conditions over SE China.

Much effort has been devoted to studying the development of spring drought conditions over SE China with a focus on precipitation. El Niño-Southern Oscillation (ENSO) is a powerful modulator of the precipitation in southern China (Wang et al. 2000; You and Jia 2018; Jia et al. 2019; Xu et al. 2021). In La Niña years, the anomalous cyclonic circulation over the western North Pacific can lead to a deficiency of spring precipitation by weakening the warm and moist southwesterlies and the water vapor convergence over SE China (Li et al. 2010; Sun and Yang 2012; Park et al. 2020). These southwesterlies may be also modulated by the snow cover and thermal forcing over the Tibetan Plateau (Wan et al. 2009; Zhang et al. 2022) and by the thermal contrast between land and oceans (Tian and Yasunari 1998; Zhao et al. 2009). In other words, the lower-tropospheric southwesterlies and horizontal moisture transport are crucial for transporting abundant moisture to SE China (Wu et al. 2012). In addition, the spring precipitation deficiency may also be driven by the anomalous descending motions modulated by the convergence anomalies at the upper troposphere, which affected by the weakened or southward-shifted East Asian subtropical jet (Wen et al. 2007; Deng et al. 2014; Jia et al. 2020). The descending motions may also be related to the local meridional circulation over the western Pacific associated with the heating in the Maritime Continent (Qiang and Yang 2013; Li et al. 2016) or an anomalous cross-equatorial vertical circulation induced by the positive sea surface temperature (SST) anomalies in the southern Indian Ocean (Jia et al. 2021).

In summary, previous studies have shown that both lower-tropospheric moisture convergence and vertical motions are important for the spring precipitation in SE China. Moreover, the lower-tropospheric moisture convergence is not only modulated by horizontal wet air advection, but also modulated by vertical motions. Thus, the

roles of horizontal wet air advection and vertical motions in spring precipitation deserve further investigations. Furthermore, vertical motions are also affected by the precipitation itself. The precipitation-associated diabatic heating can induce ascending motions and thus affect the lower-level circulation, which in turn change atmospheric moisture transportation (Sampe and Xie 2010; Wang et al. 2021). Thus, the dry dynamics that affect vertical motions should be further investigated to clarify the modulation of large-scale atmospheric circulation on vertical motions.

In this study, we investigate the drought conditions in SE China in early spring. The relative contributions of precipitation and PET to the drought conditions are quantified on interannual and long-term time scales. The dominant processes for moisture budget and vertical motions are also identified. Furthermore, we discuss the performance of these dominant processes in the drying trends over SE China.

The remainder of this paper is organized as follows. Section 2 describes the data and methodology used in this study. Section 3 quantifies the contributions of precipitation and PET to the interannual variability and long-term trend of the drought conditions over SE China in early spring. The key dynamical processes for the vertical motions and moisture transport in the drought conditions are also diagnosed in Sect. 3. The main findings are summarized and discussed in Sect. 4.

## 2 Data and methodology

### 2.1 Datasets

The monthly mean sea level pressure and geopotential height, horizontal winds, vertical velocity, air temperature, and specific humidity from 1000 to 100 hPa are obtained from the European Centre for Medium-range Weather Forecasts fifth major global reanalysis (ERA5) with a horizontal resolution of  $1.0 \times 1.0^\circ$  (Hersbach et al. 2020).

Monthly precipitation, air temperature, maximum and minimum temperatures, wind speed, relative humidity, and sunshine hours for 1979–2020 were collected from 825 meteorological stations from the National Climate Center of the China Meteorological Administration (<http://www.cma.gov.cn/en2014/>). There are 215 stations in SE China ( $20\text{--}30^\circ\text{N}$ ,  $105\text{--}123^\circ\text{E}$ , red box in Fig. 1a). Spatial interpolations of these gauge data were performed using an inverse-distance weighting method to correspond to the reanalysis data with a horizontal resolution of  $1.0 \times 1.0^\circ$ . In this study, we define the early spring as the months from February to April (FMA).

## 2.2 Standardized precipitation and evapotranspiration index

In this study, we focus on the variations of meteorological drought conditions, which are caused by a deficiency of precipitation and other meteorological conditions related to atmospheric water demand, such as high temperatures and desiccating winds (Palmer 1965). Thus, drought conditions are estimated based on the surface water balance between water supply (i.e., precipitation) and demand (i.e., PET). Precipitation can be obtained directly from observational data, while the PET needs to be estimated. Previous studies emphasize that the physically realistic PET formulations (e.g., the FAO Penman–Monteith equation) in conjunction with the abundance of in situ data sources, which are better for estimating the drought variations and its relationship with climate change (Trenberth et al. 2014). Therefore, the Penman–Monteith equation is used in this study (Allen et al. 1998):

$$PET = \frac{0.408\Delta(R_n - G) + \gamma \frac{900}{T_2 + 273} U_2 (e_s - e_a)}{\Delta + \gamma(1 + 0.34U_2)} \quad (1)$$

where  $R_n$  is the difference between the incoming net short-wave radiation and the outgoing net longwave radiation (unit:  $\text{MJ m}^{-2} \text{ day}^{-1}$ ), which is estimated by the actual duration of sunshine.  $\gamma$  is psychrometric constant (unit:  $\text{kPa } ^\circ\text{C}^{-1}$ );  $\Delta$  is the slope vapor pressure curve (unit:  $\text{kPa } ^\circ\text{C}^{-1}$ ), and  $G$  is the soil heat flux density (unit:  $\text{MJ m}^{-2} \text{ day}^{-1}$ ) and is usually set as 0 at longer time scale (e.g., monthly).  $T_2$  is the mean air temperature at 2 m height (unit:  $^\circ\text{C}$ );  $U_2$  is the wind speed at 2 m height (unit:  $\text{m s}^{-1}$ );  $e_a$  is the measured vapor pressure (unit: kPa) and  $e_s$  is the saturation vapor pressure (unit: kPa). For more descriptions about these variables, one may refer to Allen et al. (1998).

The climatology and variance of seasonal surface water balance (precipitation minus PET) are highly different between humid and relatively arid regions, or between wet and dry seasons. Hence, they need to be standardized by calculating the standardized precipitation evapotranspiration index (SPEI). Following the procedure of Vicente-Serrano et al. (2010), we calculate the probability of accumulated water balance according to a three-parameter log-logistic distribution. Stagge et al. (2015) has discussed the applicability of this probability distribution and parameter estimation. We calculate the SPEI at 3-month time scale (SPEI-3) to estimate the drought conditions, which benefits for capturing the drought conditions at seasonal time scale. The SPEI at one month (SPEI-1) is also used to reveal the annual cycle and subseasonal characteristics of the drought conditions.

In this study, the drought conditions in early spring are estimated by April SPEI-3, which is calculated based on

early-spring accumulated water balance in FMA. Additionally, we employ the standardized precipitation index (McKee et al. 1993), another well-known drought index, to emphasize the dominant role of precipitation in the drought conditions over SE China. The calculation procedures are similar with those for the SPEI, but solely dependent on precipitation and use a Pearson III distribution to calculate the probability of accumulated precipitation. The complete calculation procedures of SPI and SPEI are available in Vicente-Serrano (2006) and Vicente-Serrano et al. (2010), respectively. The SPEI and SPI were multiplied by  $-1$  in this study to facilitate the analysis of the drought conditions.

## 2.3 Attribution method

Drought conditions are caused by the variability of both precipitation and PET, but these two factors are not independent from each other. In order to quantify their respective contributions, we use an attribution method based on a series of numerical experiments following Du et al. (2019; 2021). The fundamental hypothesis of this method is that the anomalous SPEI-3 is jointly caused by the driving factors and thus equals to their linearly accumulative contributions. This method includes two procedures. First, we recalculate the SPEI-3 using a series of combinations of input variables based on observations and climatology, and construct an equation set according to the difference in those SPEI-3 results (see Fig. S1c). Then, by solving the equation set, we can determinate every section of the effects shows in Fig. S1a. Thus, the individual effect of each variable, the interaction effect among the variables, and their total effect on SPEI-3 anomalies can all be quantified (Fig. S1b). With this method, we can also quantify the effects of precipitation and PET on the long-term trend of SPEI-3 by using the detrended input variables, instead of the climatology, and construct the equation set according to the difference in SPEI-3 trend slopes (see Fig. S1d). In this study, the ‘‘Sen’s slope’’ method (Sen 1968) is applied to detect time-series trend, as it does not require a specific sample distribution nor it is influenced by outliers. The significance of the trend is examined further based on the nonparametric Mann–Kendall (MK) method (Mann 1945; Kendall 1975).

## 2.4 Moisture budget and omega equation diagnosis

We perform a moisture budget analysis to quantify the contributions of the horizontal wet air advection and the vertical transport of moisture to the drought conditions. As in previous studies (Chou et al. 2013; Li et al. 2017; Oueslati et al. 2019), moisture budget is diagnosed as follows:

$$P' = -\frac{1}{g} \int_{p_s}^{p_T} \left( \bar{V}_h \cdot \nabla_h q' \right) dp - \frac{1}{g} \int_{p_s}^{p_T} \left( \bar{V}_h' \cdot \nabla_h \bar{q} \right) dp \tag{2}$$

$$- \frac{1}{g} \int_{p_s}^{p_T} \left( \bar{\omega} \partial_p q' \right) dp - \frac{1}{g} \int_{p_s}^{p_T} \left( \omega' \partial_p \bar{q} \right) dp + E' + \delta'$$

where overbars indicate the climatology from 1979 to 2020, and primes indicate the departures from the climatology.  $P$  represents precipitation,  $E$  evaporation,  $q$  specific humidity,  $\omega$  the vertical pressure velocity, and  $\bar{V}_h$  the horizontal wind vector.  $g$  represents gravitational acceleration,  $p_s$  denotes surface pressure and  $p_T$  is the pressure of the tropopause, taken as 100 hPa. The residual term  $\delta'$  involves transient and nonlinear processes.

The first and second terms on the right-hand side of Eq. (2) represent the horizontal moisture advection anomalies induced by anomalous water vapor or anomalous horizontal velocity. The third and fourth terms represent the vertical moisture advection anomalies induced by anomalous water vapor or anomalous pressure velocity, respectively. The residual term  $\delta'$  involves transient and nonlinear processes.

To further clarify the mechanisms for the anomalous descending motion, we analyze the related dynamics through diagnosing the linearized omega equation as follows (Hu et al. 2017; Wei et al. 2017; Liu et al. 2019):

$$\omega'_D = \left( \nabla^2 + \frac{f^2}{\sigma} \frac{\partial^2}{\partial p^2} \right)^{-1} \frac{f}{\sigma} \frac{\partial}{\partial p} \left[ u' \frac{\partial \bar{\zeta}}{\partial x} + v' \frac{\partial \bar{\zeta}}{\partial y} + \bar{u} \frac{\partial \zeta'}{\partial x} + \bar{v} \frac{\partial \zeta'}{\partial y} \right]$$

$$+ \left( \nabla^2 + \frac{f^2}{\sigma} \frac{\partial^2}{\partial p^2} \right)^{-1} \frac{R}{\sigma p} \nabla^2 \left[ u' \frac{\partial \bar{T}}{\partial x} + v' \frac{\partial \bar{T}}{\partial y} + \bar{u} \frac{\partial T'}{\partial x} + \bar{v} \frac{\partial T'}{\partial y} \right]$$

$$= \omega'_A + \omega'_B = \omega'_{A1} + \omega'_{A2} + \omega'_{A3} + \omega'_{A4} + \omega'_{B1} + \omega'_{B2} + \omega'_{B3} + \omega'_{B4} \tag{3}$$

where overbars indicate the climatology from 1979 to 2020, and primes indicate the departures from the climatology.  $f$  denotes the Coriolis parameter,  $u$  the zonal wind, and  $v$  the meridional wind.  $\zeta$  denotes the vertical component of relative vorticity.  $\sigma = R/[RT/c_p p] - (\partial T/\partial p)$  represents the

background static stability;  $R = 287 \text{ J kg}^{-1} \text{ K}^{-1}$  represents the gas constant for dry air;  $c_p = 1004 \text{ J kg}^{-1} \text{ K}^{-1}$  is the specific heat of dry air at constant pressure. The vertical velocity anomalies are induced by the vertical gradient of horizontal vorticity advection and the horizontal temperature advection, marked as terms A and B, respectively.

### 3 Results

#### 3.1 Early spring drought conditions over SE China

The early spring (FMA) is a transitional period from dry to wet conditions (Fig. 2a). Following the dry season, the droughts in early spring may lead to more destructive conditions due to the cumulative effect of drought. Figure 2b shows that significant drying trends in the SPEI-1 appear in February and April over SE China. The strongest drying trend in the SPEI-3 is about 0.22 per decade, which appears in April (Fig. 2b). The spatial distribution of the April SPEI-3 also shows significant drying trends over SE China in early spring from 1979 to 2020 (Fig. 3a). The most obvious drying trend is more than 0.3 decade<sup>-1</sup> in the southeast coastal region (Fig. 3a). These results indicate that the drying conditions are severe in early spring and last from February to April over SE China.

Drought conditions are associated with precipitation and PET. On interannual time scale, regressed FMA-accumulated precipitation and PET against the April SPEI-3 show that both precipitation deficiency and increased PET are significantly related to the drought conditions (Figs. 4a, b). Besides, the correlation coefficient between the detrended SPEI and SPI is 0.98, indicating the important role of precipitation in the drought conditions on interannual time scale. Due to the non-independence between precipitation and PET, we apply a new attribution method developed by Du et al. (2019, 2021) to quantify the contributions of

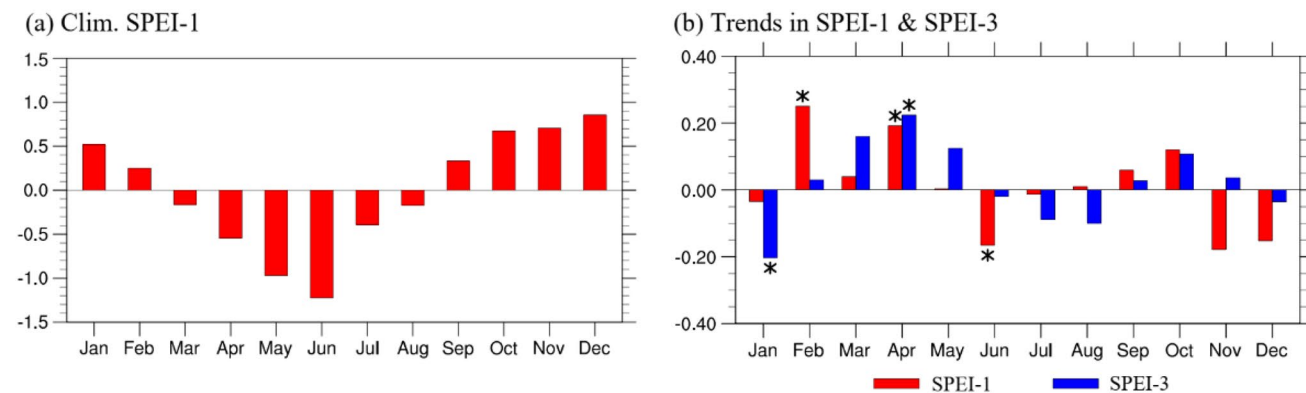


**Fig. 2** **a** The annual cycle of monthly mean of SPEI-1 over SE China. **b** The annual cycle of the linear trends of SPEI-1 and SPEI-3 over SE China. The significant values of trends exceeding the 0.05 significance level are indicated by asterisks

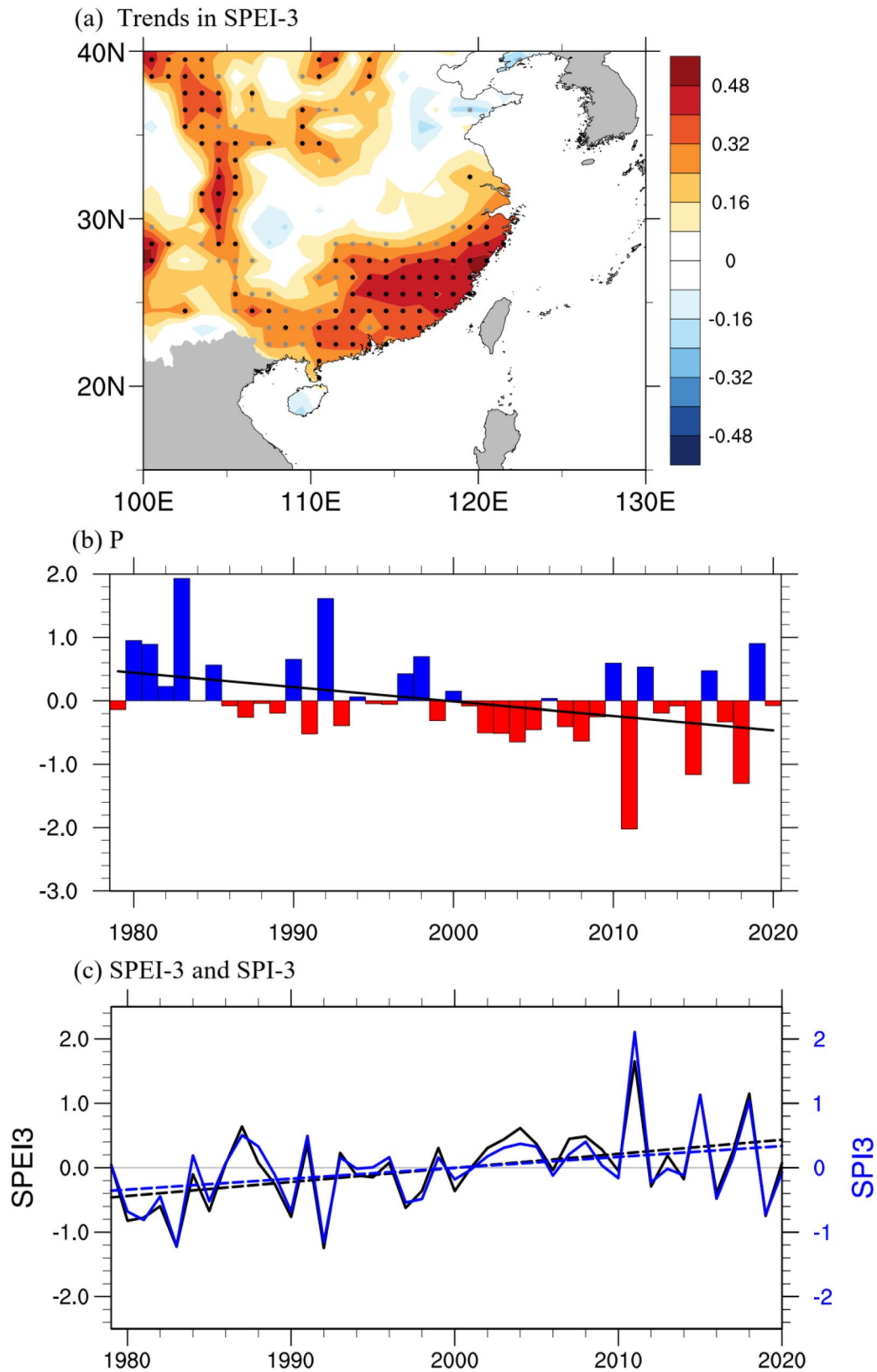


**Fig. 3** **a** Spatial distributions of the linear trend of April SPEI-3 (unit: decade<sup>-1</sup>). Significant values exceeding the 0.1 and 0.05 significance levels are marked by gray and black dots, respectively; **b** Time series of FMA-accumulated precipitation averaged over SE China (unit: mm

day<sup>-1</sup>). Black solid line indicates the linear trend of precipitation; **c** is the same as **b**, but for April SPEI-3 (black line) and SPI-3 (blue line). Black and blue dashed lines indicate the linear trends in April SPEI-3 and SPI-3, respectively

precipitation and PET on the drought conditions. Precipitation contributes more than 90% of the April SPEI-3 variability over SE China, while PET contributes less than 10% (Fig. 4c, d). The domain average contributions of precipitation and PET over SE China are 96.5% and 6.7%, respectively. The interaction between precipitation and PET contributes  $-3.2\%$ . These results indicate that precipitation deficiency is the dominate factor for the interannual variability of drought conditions even in the transitional season.

For the long-term trend, most of SE China has suffered from significantly decreased precipitation and increased PET during 1979–2020 (Fig. 5a, b). The long-term trend in the decreased precipitation over SE China is  $-0.23 \text{ mm day}^{-1} \text{ decade}^{-1}$ , which is larger than the increased PET ( $0.10 \text{ mm day}^{-1} \text{ decade}^{-1}$ ). Furthermore, the April SPI-3 (Fig. 3c, blue line)

shows a significant positive tendency of  $0.17 \text{ decade}^{-1}$ , which is comparable to that of SPEI-3 (Fig. 3c, black line,  $0.22 \text{ decade}^{-1}$ ). According to the attribution method developed by Du et al. (2019, 2021), the contribution of the decreased precipitation accounts for 72.8% of the decreasing trend of April SPEI-3 (Fig. 5c), and the contribution of PET is 22.3% (Fig. 5d). It may be caused by the accumulated rainfall deficiency and water demand from winter to spring. Although the decreased precipitation still plays a primary role in controlling the drying trend, the contribution of PET to the drying trend (22.3%) is much larger than that to the interannual variability of early spring drought conditions (6.7%). The increasing trend of PET is dominated by the warming surface air, which contributes about 60.0% of the trend (Fig. S6). This feature implies the change in PET cannot be neglected in the future

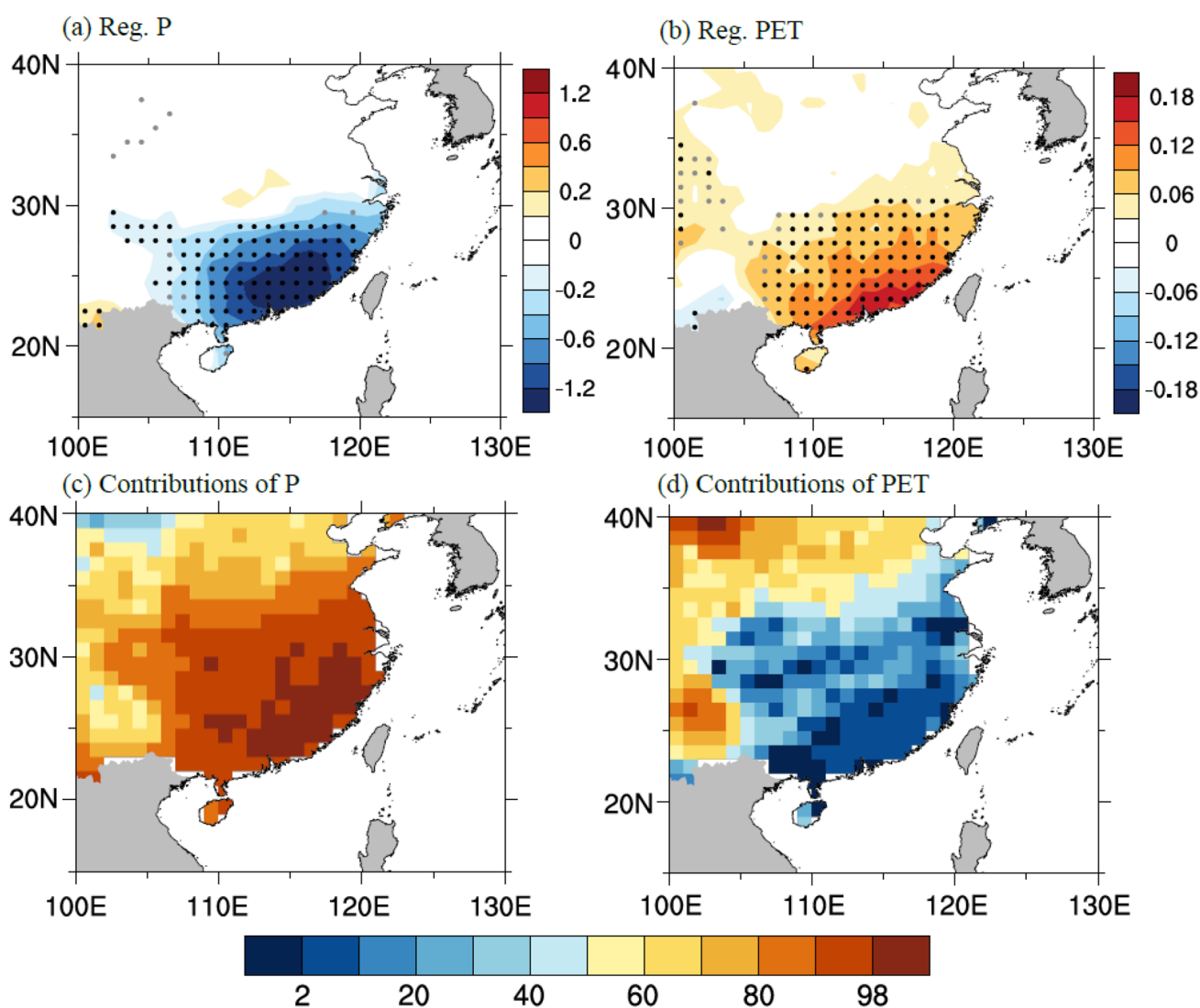


**Fig. 4** Regression of detrended **a** precipitation and **b** PET onto the detrended SPEI-3 over SE China (unit:  $\text{mm day}^{-1}$ ). Significant values exceeding the 0.1 and 0.05 significance levels are marked by gray and

black dots, respectively. Contributions of **c** precipitation and **d** PET to the April SPEI-3 (unit: %) at interannual time scale are also shown

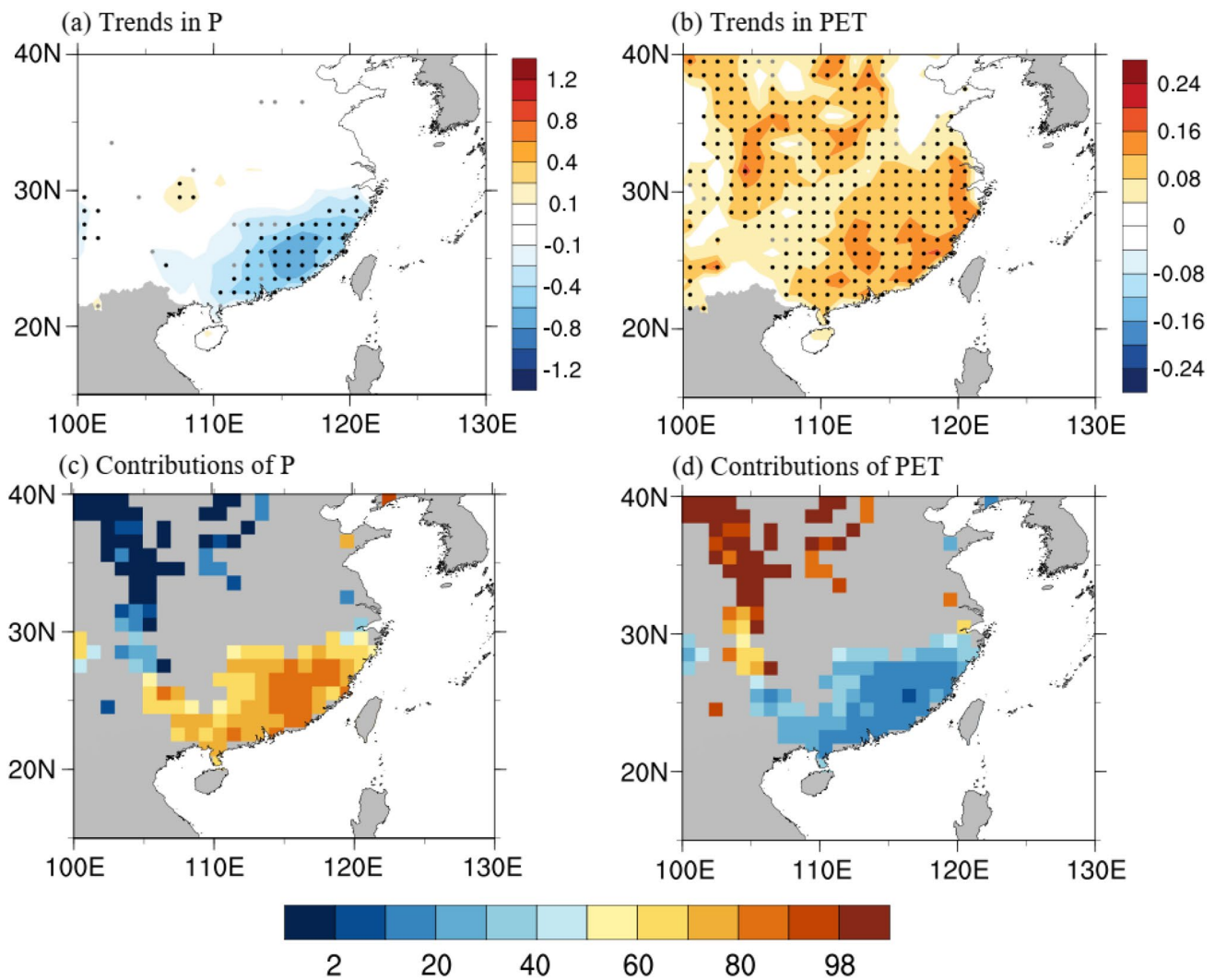


**Fig. 5** The linear trend of **a** FMA-accumulated precipitation (unit:  $\text{mm day}^{-1} \text{decade}^{-1}$ ) and **b** FMA-accumulated PET (unit:  $\text{decade}^{-1}$ ). Significant values exceeding the 0.1 and 0.05 significance levels are marked by gray and black dots, respectively. The contributions of **c**

**P** and **d** PET to the linear trend of April SPEI-3 (unit: %) are also calculated, but only the regions with the linear trend of April SPEI-3 exceeding the 0.1 significance level are shown

change in early spring drought conditions in a warming climate. Following the significantly increasing temperature in a warming climate, the PET may tend to increase and contribute to the worse drought conditions. Moreover, the meteorological drought tendency in both the last century and the end of the twenty-first century strongly depends on whether PET is included as a climate driver (Vicente-Serrano et al. 2010; Cook et al. 2014; Spinoni et al. 2020). Thus, it is necessary to consider the role of the PET in the change in drought conditions over SE China in the future. However, the drying trend is still dominated by the decreased precipitation over SE China in the recent decades.

### 3.2 Dynamical processes for interannual variability of drought

The drought conditions in early spring in SE China is dominated by the precipitation deficiency, which may be caused by the moisture deficiency in the atmospheric column and descending motions over SE China (Qiang and Yang 2013; Hu et al. 2017). Climatologically, SE China is dominated by westerlies in early spring (Fig. S2a and S2c), and the associated moisture convergence and ascending motions are conducive to increased precipitation over SE China (Fig. S2b and S2d). However, in the drought condition, SE China is controlled by a barotropic high anomaly over the eastern TP (Fig. 6a, c), which prohibits the ascending motions over SE China (Fig. 6d and Fig. S2d). The anomalous descending



motions could provide an unfavorable dynamic condition for precipitation by suppressing the vertical convection. Meanwhile, they could also provide an unfavorable moisture environment for precipitation by weakening the vertical transport of moisture and leading to moisture divergence anomalies (Fig. 6b). Accompanying with the high anomaly over the eastern TP, intense northeasterly anomalies appear along its eastern flank between this anomalous high and the anomalous low pressure over the western North Pacific, where the height gradient is strong. The intense northeasterly anomalies may prevent wet air flow from the lower latitudes to SE China and benefit moisture divergence anomalies. Significant moisture divergence can be observed over SE China and the northern South China Sea (Fig. 6b). Besides, the northeasterly anomalies may lead to the cold advection to SE China, which is unfavorable for the ascending motion in situ (Fig. 6d). However, does the horizontal wet air advection or the vertical motion play a more important role in the

moisture divergence anomalies? To quantify the contributions of these two factors on the moisture divergence anomalies, we perform a moisture budget analysis.

Figure 7a shows that the precipitation deficiency over SE China is mainly induced by negative vertical moisture advection anomalies as supported by the anomalous descending motions. These anomalous descending motions appear throughout the troposphere with peak values around 500 hPa in the middle troposphere (Fig. 7b). These features are generally consistent with those of the study by Li et al. (2017) on spring persistent precipitation over SE China. Besides, the negative horizontal moisture advection associated with horizontal wind anomalies also dries out the troposphere by transporting dry air into SE China, but this effect is much smaller compared to the vertical moisture advection. The contribution of evaporation is also negligible. Moreover, the correlation coefficients of the SPEI-3 with the precipitation and the vertical motion

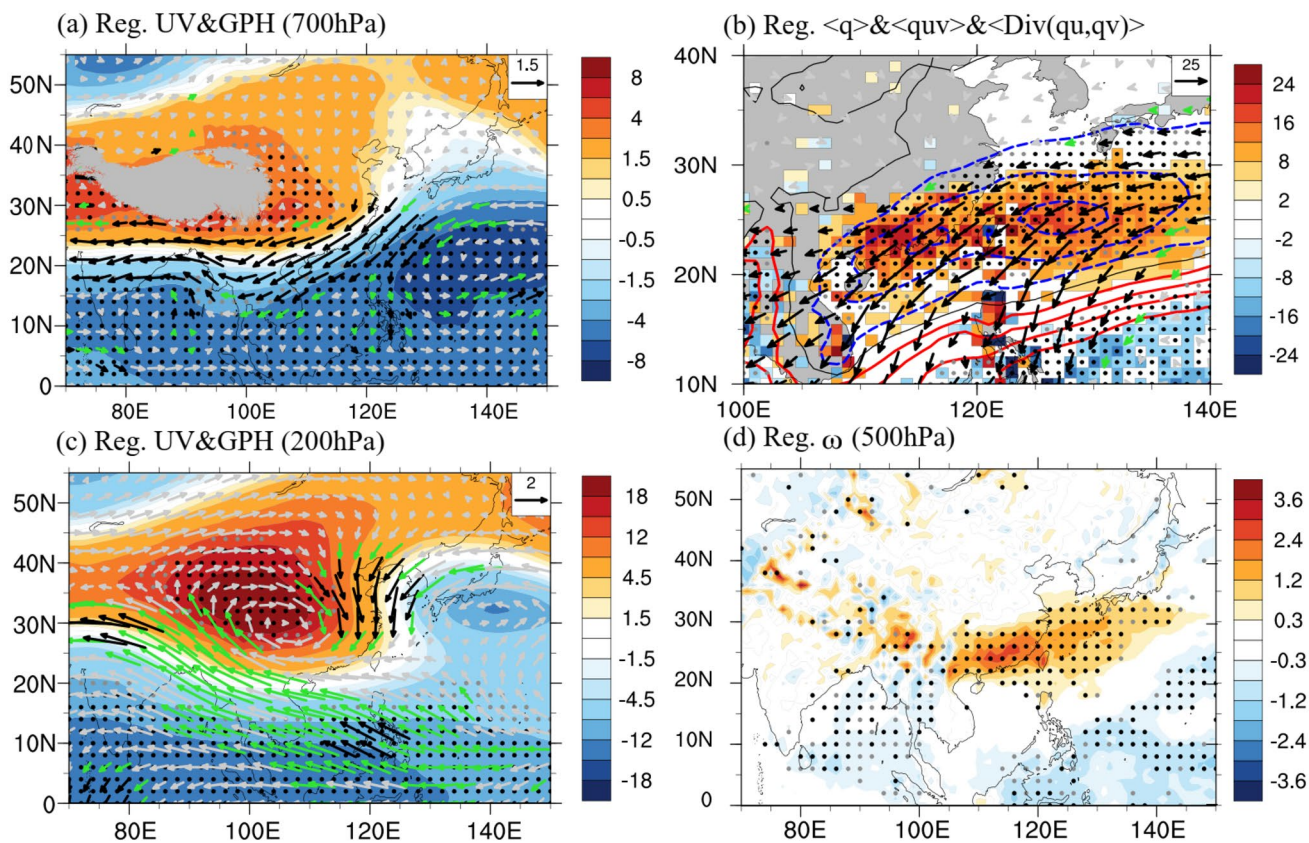
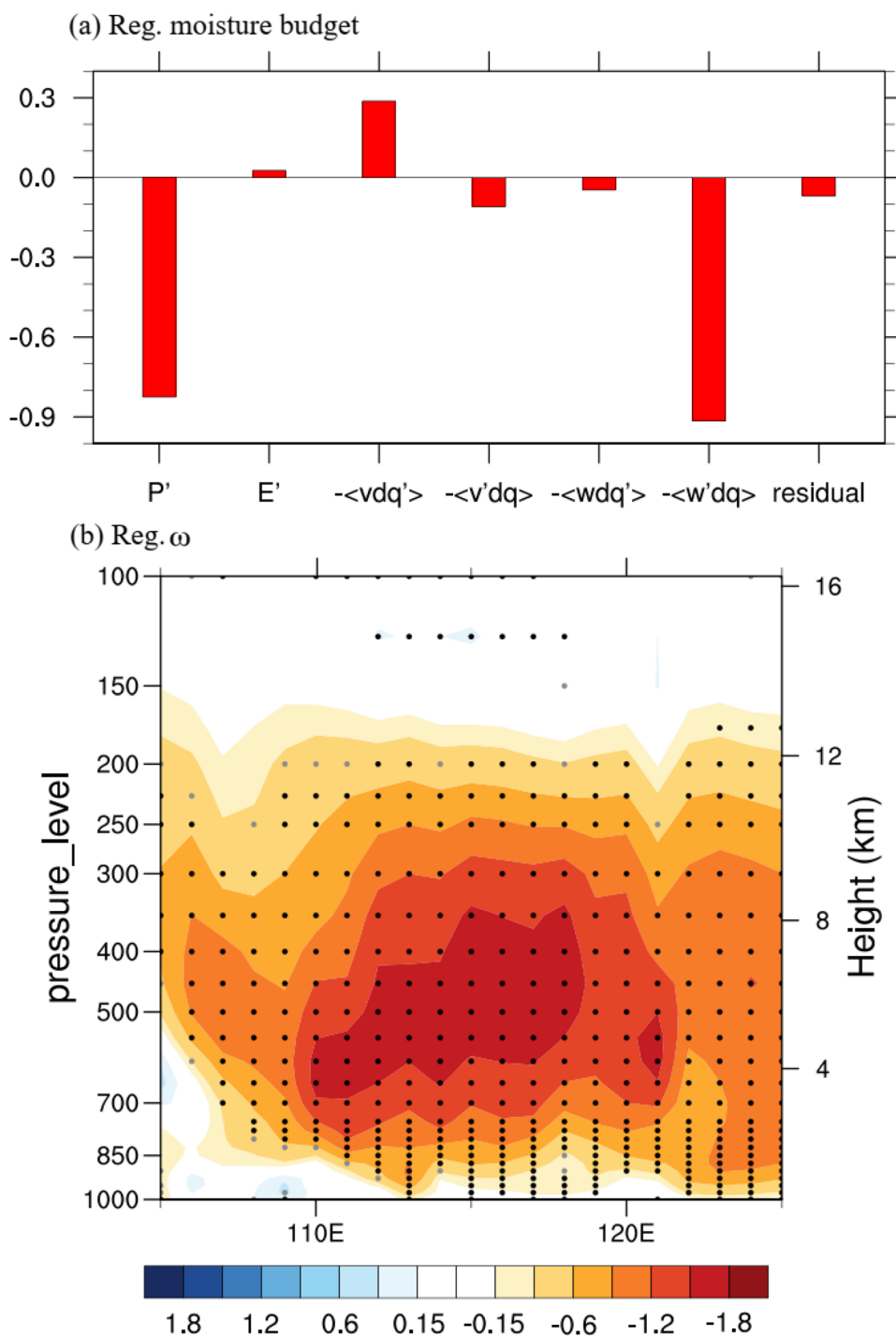


**Fig. 6** Regression of detrended variables onto the detrended SPEI-3 over SE China. **a** is for horizontal wind (vectors; unit:  $m s^{-1}$ ) and geopotential height (shading; unit: m) at 700 hPa, **b** is for vertical integral of specific humidity (contours; unit:  $kg m^{-2}$ ), and vertical integral of water vapor flux (vectors; unit:  $kg m^{-1} s^{-1}$ ) as well as its divergence (shading; unit:  $kg m^{-2} s^{-1}$ ), **c** is the same as **a** except for 200 hPa, and **d** is for omega (unit:  $10^{-2} Pa s^{-1}$ ) at 500 hPa. Significant values exceeding the 0.1 and 0.05 significance levels are marked

by gray and black dots, respectively. Significant zonal or meridional values exceeding the 0.1 and 0.05 significance levels are marked by green and black vectors, respectively. The shading or contour areas of exceeding the 0.1 and 0.05 significance levels are marked by gray and black dots, respectively. Only the vertically-integrated moisture flux convergence exceeding the 0.1 significance level is plotted. The TP region with elevations exceeding 3000 m is shaded gray

**Fig. 7** **a** Regression of detrended precipitation and other components of moisture budget onto the detrended SPEI-3 over SE China (unit:  $\text{mm day}^{-1}$ ). **b** Longitude–altitude section of vertical velocity (unit:  $10^{-2} \text{ Pa s}^{-1}$ ) averaged between 21 and 29 °N, in which the significant values exceeding the 0.1 and 0.05 significance levels are marked by gray and black dots, respectively



induced vertical moisture advection anomalies over SE China are 0.91 and 0.88, respectively. The descending motion anomalies are dominant in the precipitation deficiency and drought conditions in early spring.

The linearized omega equation is diagnosed to clarify the dynamics for the anomalous descending motion. Figure 8 shows that term B ( $\omega'_B$ , black solid line), the horizontal temperature advection, is more important in the lower

troposphere, but term A ( $\omega'_A$ , red solid line), the vertical gradient of horizontal vorticity advection, is more important in the upper troposphere. Especially,  $\omega'_{A3}$  and  $\omega'_{B2}$  are the dominant terms responsible for anomalous descending motions, which further lead to the early spring drought-prone conditions over SE China. Moreover, we quantify the contributions of individual term by calculating the vertical-averaged vertical velocity anomalies from surface pressure to 200 hPa

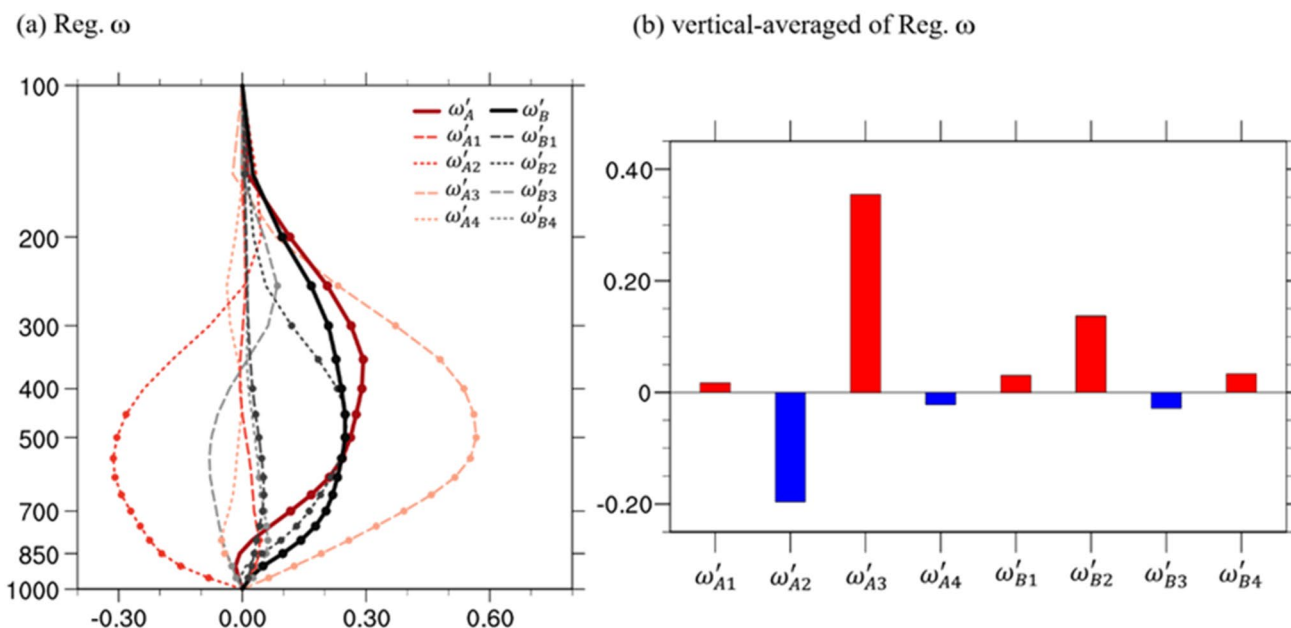


**Fig. 8** **a** Vertical profiles of the regression of detrended omega (unit:  $10^{-2} \text{ Pa s}^{-1}$ ) and its components (unit:  $10^{-2} \text{ Pa s}^{-1}$ ) onto the detrended SPEI-3 over SE China. Dots on lines indicate the significant values

exceeding the 0.05 significance level. **b** The vertical averages of various omega components in the troposphere

(Fig. 8b). The vertical-averaged  $\omega'_{A3}$  is  $0.35 \cdot 10^{-2} \text{ Pa s}^{-1}$ , contributing about 108.8% of the dry-dynamics-related descending motion anomalies. The positive contribution of these terms is partially offset by the negative contribution of the terms  $\omega'_{A2}$ ,  $\omega'_{A4}$ , and  $\omega'_{B3}$ . On the other hand, the vertical-averaged  $\omega'_{B2}$  is  $0.14 \cdot 10^{-2} \text{ Pa s}^{-1}$ , accounting for about 42.0% of the dry-dynamics-related descending motion anomalies.

The term  $\omega'_{A3}$  is the primary term responsible for the anomalous descending motion below 200 hPa. It is closely related to the vertical gradient of the anomalous vorticity advection  $-\bar{u} \left( \frac{\partial \zeta'}{\partial x} \right)$  induced by the variation of zonal vorticity gradient. As shown in Fig. 9a, associated with the early spring drought-prone conditions over SE China, there is a large positive vertical gradient of horizontal vorticity advection (Fig. 9a, black line). The related circulations and dynamical processes are further investigated. In Fig. 9c and d, a barotropic anticyclonic anomaly dominates over the eastern TP, which leads to positive zonal vorticity gradient anomalies over SE China, with a slight variation in the troposphere (Fig. 9a, blue line). Besides, the climatology of 200-hPa zonal wind features the spring East Asian subtropical jet (EASJ) over SE China (Fig. 9b, shading). Accompanying the positive zonal vorticity gradient anomalies, the westerly wind leads to negative anomalous vorticity advection throughout the troposphere. Furthermore, the vertical shear of the westerly wind is strong beneath the jet since the westerly wind is much weaker in the lower troposphere than in the upper troposphere (Fig. 9a, red line). This strong vertical

shear of westerly wind drives the evident vertical gradient of negative anomalous vorticity advection, which peaks in the upper troposphere and is close to zero in the lower troposphere. These configurations create strong positive vertical gradient of horizontal vorticity advection  $-\bar{u} \left( \frac{\partial \zeta'}{\partial x} \right)$  (Fig. 9a, black line), which could lead to anomalous descending motions over SE China.

The term  $\omega'_{B2}$  is the second-most significant term responsible for the anomalous descending motions, and it is closely related to the anomalous horizontal temperature advection  $-v' \left( \frac{\partial \bar{T}}{\partial y} \right)$  induced by the variation of meridional wind. As shown in Fig. 9b, there are significant cold advection anomalies throughout the troposphere over SE China (black line). A further investigation onto the related dynamical processes shows that SE China is controlled by the significant northerly anomalies throughout the troposphere (Fig. 9b, blue line), which is dominated by a barotropic anticyclonic anomaly over the eastern TP and an anomalous cyclone over the western North Pacific (Fig. 6a and c). Additionally, the climatology of meridional temperature gradient is negative below 200 hPa over SE China. These configurations create significant cold advection (Fig. 9b, black line), which could induce anomalous descending motions over SE China.

These results emphasize the dominant roles of vertical motions and the associated vertical moisture advection in the interannual variability of early spring drought conditions over SE China. The anomalous descending motions benefit from the atmospheric circulation pattern with a barotropic

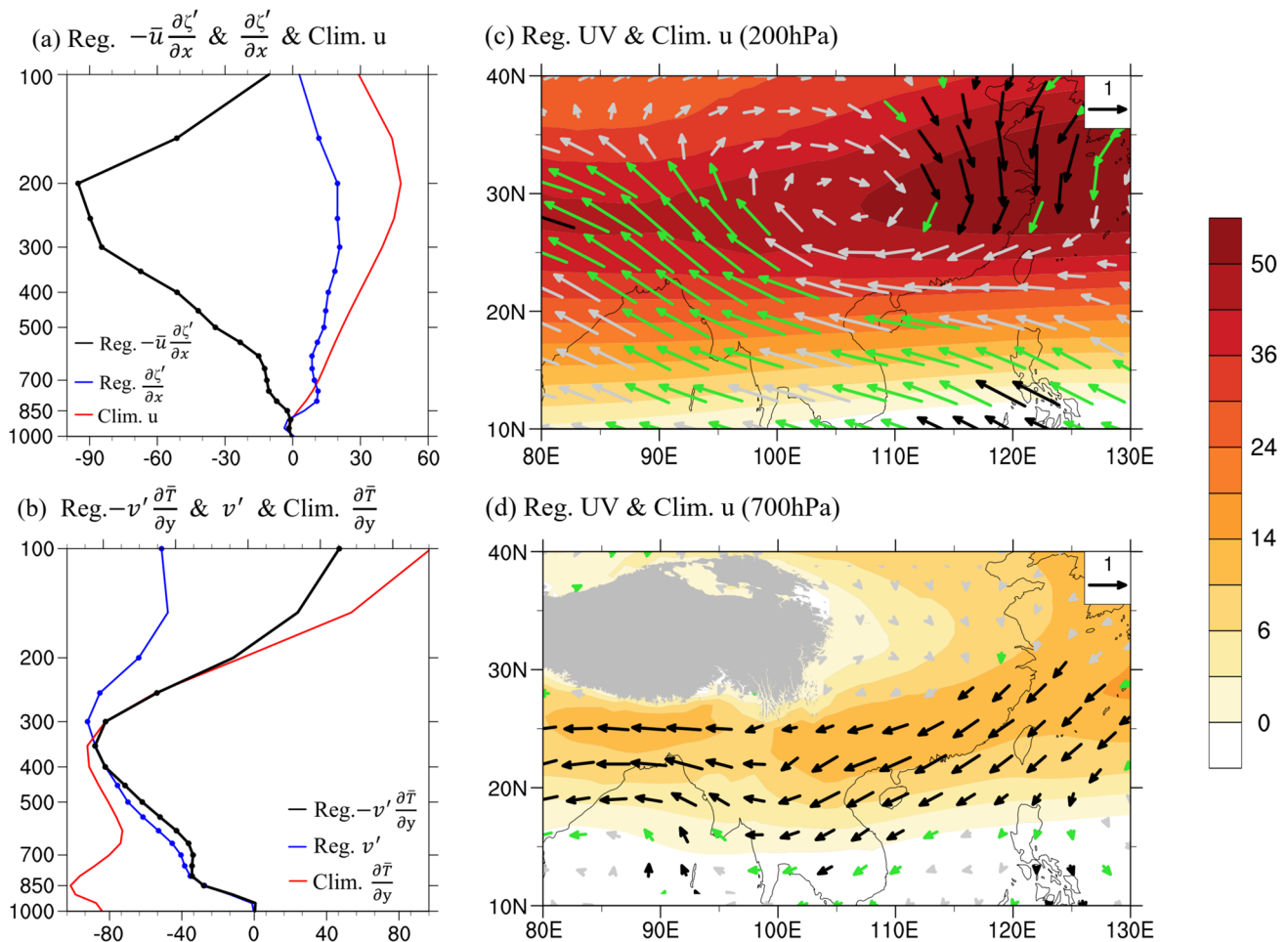


**Fig. 9** **a** Vertical profiles of the climatology of zonal wind (red line; unit:  $\text{m s}^{-1}$ ) and the regression of detrended vorticity advection  $-\bar{u}(\partial\zeta'/\partial x)$  (black line; unit:  $10^{-12} \text{ s}^{-2}$ ) and zonal vorticity gradient  $\partial\zeta'/\partial x$  (blue line; unit:  $10^{-13} \text{ m}^{-1} \text{ s}^{-1}$ ) onto the detrended SPEI-3 over SE China. **b** is same as **a**, but for the climatology of meridional temperature gradient  $\partial\bar{T}/\partial y$  (red line; unit:  $10^{-7} \text{ m}^{-1} \text{ s}^{-1}$ ) and the regressed meridional temperature advection  $-v'(\partial\bar{T}/\partial y)$  (black line; unit:  $10^{-7} \text{ s}^{-2}$ ) and the regressed meridional wind  $v'$  (blue line; unit:  $10^{-2} \text{ m s}^{-1}$ ). Dots indicate signifi-

cant values exceed the 0.1 significance level. **c** Regression of detrended horizontal wind (vectors; unit:  $\text{m}^{-1} \text{ s}^{-1}$ ) onto the detrended SPEI-3 over SE China and the climatology of zonal wind (shading; unit:  $\text{m}^{-1} \text{ s}^{-1}$ ) at 200 hPa. **d** is same as **c**, but at 700 hPa. Significant zonal wind or meridional wind exceeding the 0.1 and 0.05 significance levels are marked by green and black vectors, respectively. The Tibetan Plateau region with elevations exceeding 3000 m is shaded gray

anomalous anticyclone over the eastern TP and an anomalous cyclone over the western North Pacific. This circulation pattern favors the negative zonal vorticity advection and the cold advection over SE China in early spring, leading to the anomalous descending motions and resulting in the drought conditions over SE China.

Several mechanisms have been suggested for these large-scale circulation anomalies. The anomalous cyclone over the western North Pacific is considered to be associated with La Niña (Wang et al. 2000; Gao and Yang 2009; Xie et al. 2016; Li et al. 2022). The regressed SST anomalies onto the April SPEI-3 of SE China appears a La Niña-like pattern with significantly negative SST anomalies in

the central eastern tropical Pacific (Fig. S3). In addition, the anomalous anticyclone over the eastern TP may also be contributed by the La Niña-like pattern through the poleward Rossby wave train associated with the heating over the Maritime Continent (Zheng et al. 2012; Abdillah et al. 2017). Moreover, the anomalous anticyclone could be contributed by the positive thermal forcing over the TP during winter and spring (Zhang et al. 2004; Duan et al. 2013; Jia et al. 2020). The warming appears over the TP land surface (Fig. S4a), which increases the upward sensible heat fluxes (Fig. S4b) and upward longwave radiation fluxes (Fig. S4c), and further leads to anomalous high pressure over the eastern TP.

### 3.3 Dynamical processes for long-term trend of drought

It is revealed above the interannual variability of drought conditions in early spring is dominated by the barotropic anomalous anticyclone over the eastern TP and an anomalous cyclone over the western North Pacific through suppressing ascending motions. This section further investigates whether these dynamic processes dominate the drying trend of drought conditions.

Result of a moisture budget diagnosis confirms that the weakened vertical moisture advection ( $\omega' \partial_p \bar{q}$ ) associated with the descending trend throughout the troposphere (Fig. 10b) dominates the drying trend over SE China (Fig. 10a). The descending trend is investigated with a linearized omega equation diagnosis. Figure 11 shows that the descending trend induced by the horizontal temperature advection ( $\omega'_B$ , black solid line), is more important in the lower troposphere, but the descending trend induced by the horizontal vorticity advection ( $\omega'_A$ , red solid line) is more important in the upper troposphere. Especially, the

descending trend is dominated by  $\omega'_{A3}$  and  $\omega'_{B2}$ . As demonstrated in Fig. 10c and d, accompanying the stronger positive trend in geopotential height surrounding the eastern TP, there is a barotropic anticyclonic anomaly over this region and northeasterly wind anomalies over SE China. This anticyclonic anomaly could induce a positive trend of zonal vorticity gradient over SE China (Fig. 11b, blue line), which in conjunction with the spring EASJ leads to the obviously decreased vertical gradient of vorticity advection (Fig. 11b, black line) and the weakened ascending motions ( $\omega'_{A3}$ ). Additionally, these northeasterly wind anomalies contribute to the significant enhanced meridional cold advection  $-v'(\partial \bar{T} / \partial y)$  (Fig. 11c, black line), which could also lead to the weakening ascending motions over SE China ( $\omega'_{B2}$ ). The contribution of latter process to the troposphere-averaged descending anomalies is  $0.08 \text{ } 10^{-2} \text{ Pa s}^{-1} \text{ decade}^{-1}$ , accounting for about 29.6% of the dry-dynamics-related descending trend, which is much weaker than the former process ( $0.23 \text{ } 10^{-2} \text{ Pa s}^{-1} \text{ decade}^{-1}$ , 85.2%). These results suggest that the barotropic anomalous anticyclone over the eastern TP and

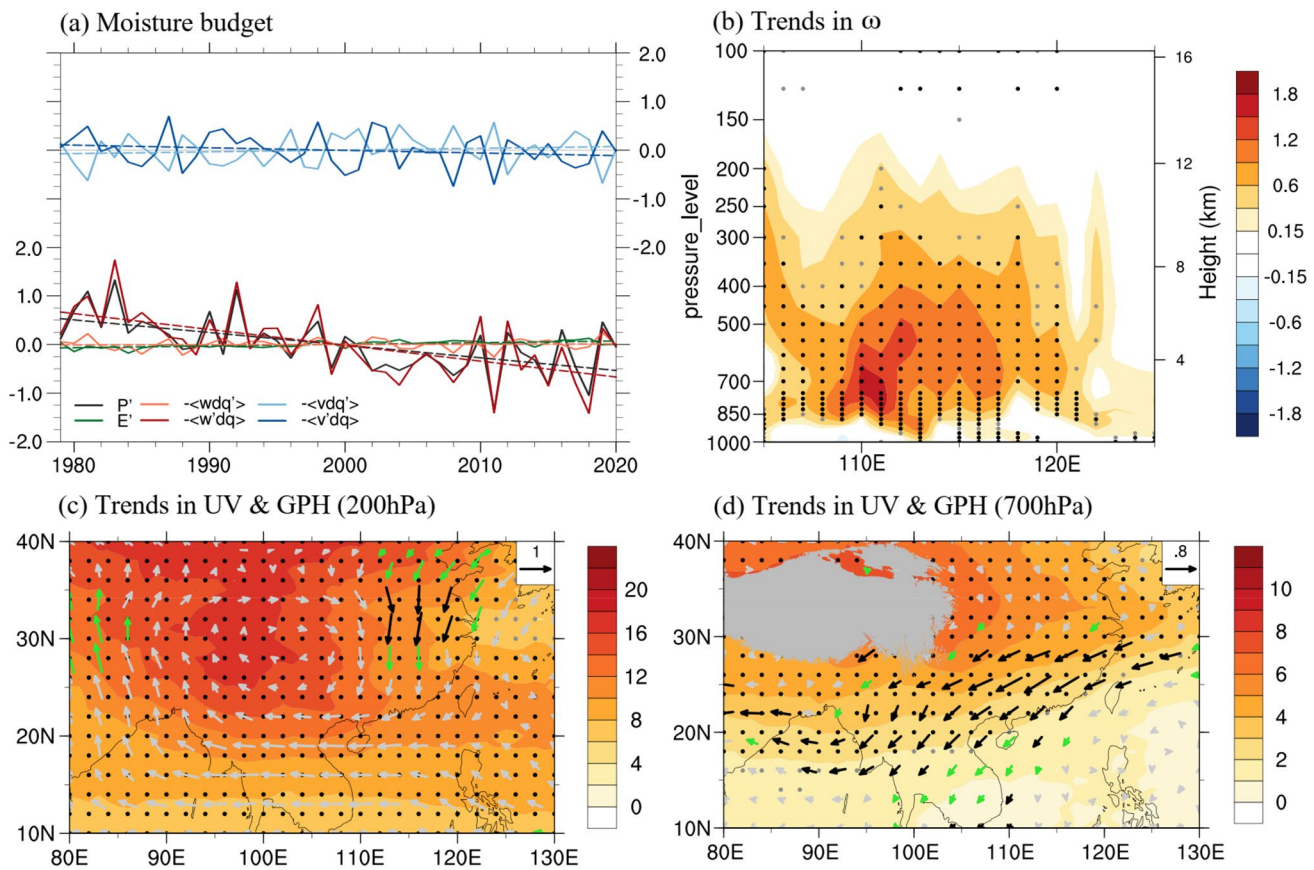


**Fig. 10** **a** Time series of precipitation and other components of moisture budget over SE China (unit:  $\text{mm day}^{-1}$ ). **b** is same as Fig. 7b, but for the linear trends in vertical velocity (unit:  $10^{-2} \text{ Pa s}^{-1} \text{ decade}^{-1}$ ). **c-d** are same as Fig. 6a and 6c, respectively, but for the linear trend

in horizontal wind (vectors; unit:  $\text{m s}^{-1} \text{ decade}^{-1}$ ) and geopotential height (shading; unit:  $\text{m decade}^{-1}$ ). The Tibetan Plateau region with elevations exceeding 3000 m is shaded gray

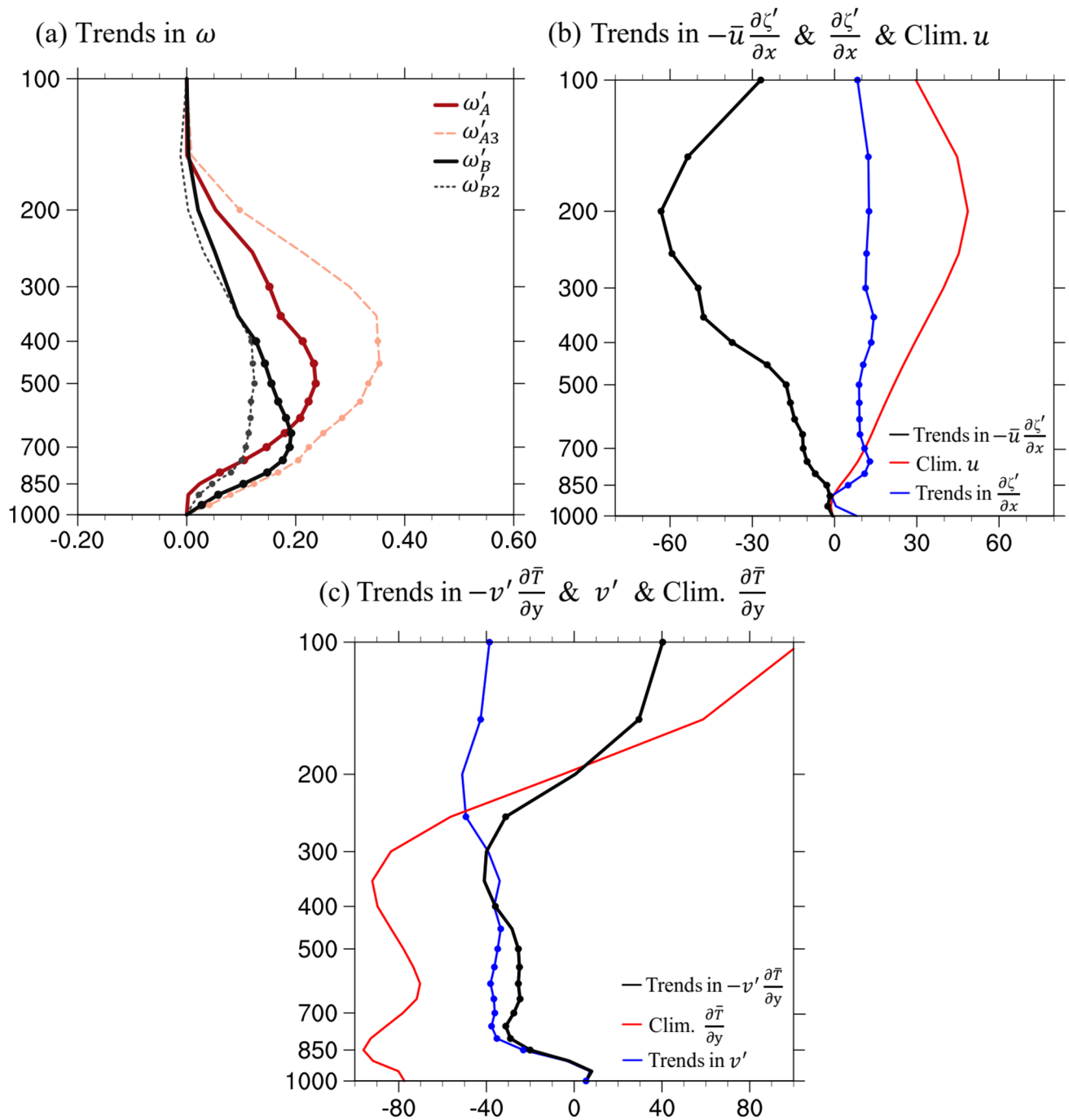


**Fig. 11** **a** is same as Fig. 8a, but for the linear trend in omega and its components (unit:  $10^{-2} \text{ Pa s}^{-1} \text{ decade}^{-1}$ ). **b–c** are same as Fig. 9a and b, respectively, but for the linear trends in **b** vorticity advection  $-\bar{u}(\partial \zeta' / \partial x)$  (black line; unit:  $10^{-12} \text{ s}^{-2} \text{ decade}^{-1}$ ) and zonal vorticity

gradient  $\partial \zeta' / \partial x$  (blue line; unit:  $10^{-13} \text{ m}^{-1} \text{ s}^{-1} \text{ decade}^{-1}$ ) and **c** temperature advection  $-v'(\partial \bar{T} / \partial y)$  (black line; unit:  $10^{-7} \text{ s}^{-2} \text{ decade}^{-1}$ ) and meridional wind  $v'$  (blue line; unit:  $10^{-2} \text{ m s}^{-1} \text{ decade}^{-1}$ )

the anomalous cyclone over the western North Pacific dominates the drying trend over SE China in early spring by leading to the weakened ascending motions and the decreased precipitation. These dynamics are responsible for the drought conditions for both the interannual variability and the long-term trend.

The strong positive trend in the geopotential height over the eastern TP may benefit from the land-atmospheric interaction. The land skin temperature strengthens rapidly in East Asia in early spring, compared with SST in the ocean (Fig. S4d), which may lead to the rapid increases in upward sensible heat and longwave radiation fluxes (Figs. S4e and

S4f). These features can induce a rapidly warming in the troposphere and a strong positive geopotential height with the center over the TP (Fig. 10c). The positive geopotential height in turn inhibits the convection in situ and further strengthens the warming. This positive feedback loop may lead to more intense and significant positive trend in the geopotential height over the TP, and result in the anticyclonic trend at the upper level (Fig. 10c). In the eastern flank of the anticyclone, the trend in the northerly wind is significant over SE China, due to the strong zonal thermal contrast between the TP and the western North Pacific. The significant northerly trend over eastern China and the anticyclonic trend over the TP can lead to the descending trend over SE China by enhancing the cold advection and the negative vorticity advection, respectively.

At the lower level, the trends in the northeasterly wind over SE China may be partially associated with the quasi-barotropic anticyclone over the TP with the northeasterly in the southeastern flank (Fig. 10c and d). Besides, the northeasterly trends may also be associated with cyclonic trend over the western North Pacific at the lower troposphere, which may intensify the northeasterly in its northwestern flank over SE China (Fig. 10d). The northeasterly trend can contribute to the cold advection over SE China and lead to the drying trend in over SE China in early spring. The cyclonic trend in the western Pacific can benefit from the warming trend in situ in early spring (Li et al. 2016, 2022).

## 4 Summary and discussions

The drought conditions in early spring and their related dynamic processes on interannual and long-term time scales are investigated for SE China. The precipitation in early spring shows a significant negative trend about  $-0.23 \text{ mm day}^{-1} \text{ decade}^{-1}$ . The precipitation deficiency dominates the variations of drought conditions over SE China and contributes about 96.5% and 72.8% of the interannual variability and the drying trend of drought conditions, respectively. On the other hand, the contribution of PET to the drying trend (22.3%) is about four times larger than that to interannual variability (6.7%). In a warming climate, the significantly increasing temperature may increase the PET and contribute to the worse drought conditions. It may play a more important role in the change in drought conditions in the future than in the recent decades. The PET amplification effect is especially pronounced in SE China and it plays a critical role in the drought tendency in the end of the twenty-first century (Cook et al. 2014).

On interannual time scale, accompanying with the precipitation deficiency over SE China, anomalous descending motions and moisture divergence appear in this region,

which provide unfavorable dynamic conditions and moisture environments for precipitation. The result from moisture budget analysis shows that weakened ascending motions and hindered ascending moisture advection play critical roles in controlling the precipitation deficiency and drought-prone conditions. Besides, a significant weakening trend of ascending motions appears throughout the troposphere over SE China, which also plays a vital role in contributing to the drying trend.

Further investigation into the vertical motions shows that the dominant dynamics responsible for the anomalous descending motions are the positive vertical gradient of zonal vorticity advection anomalies  $-\bar{u}(\partial\zeta'/\partial x)$  and the enhanced meridional cold advection  $-v'(\partial\bar{T}/\partial y)$ , which account for about 108.8% and 42.0% of the dry-dynamics-related descending motion anomalies, respectively. Additionally, the descending trend of vertical motions over SE China is also dominated by the same factors that account for about 85.2% and 29.6% of the dry-dynamics related descending trend, respectively. These factors are controlled by the barotropic anomalous anticyclone over the eastern TP and the anomalous cyclone over the western North Pacific. These circulations dominate the descending motions over SE China for both the interannual variability and the long-term trend, and result in the drought conditions in early spring in SE China.

As the interannual variability and drying trend of the drought conditions are dominated by similar atmospheric circulations and dynamics, the drying trend over SE China during recent decades may also be controlled by the internal climate variability. Further study is deserved to reveal the role of internal dynamics in the decreasing trend of precipitation in early spring over SE China. Several previous studies suggested that the negative Pacific decadal oscillation (PDO) phase and the positive Atlantic decadal oscillation (AMO) phase may drive the interdecadal decrease in spring precipitation over southern China (Wu and Mao 2016, 2018; Wen et al. 2021). From 1979 to 2020, the PDO/AMO changes from positive/negative phase to negative/positive phase (Fig. S5). The correlation coefficient between the 9-month running means of the April SPEI-3 and the PDO/AMO index is 0.88/−0.87. It indicates that the drying trend in recent decades may be part of the interdecadal change in SE China. How do AMO and PDO affect the change in drought conditions? Which one is more important? These questions need to be further investigated using climate models. Besides, it has been successfully detected that the anthropogenic forcing has increased the drought risk over Southeast Asia (including SE China), both in historical simulation and the future projection under all scenarios (Zhang et al. 2021). Further study is deserved to clarify the role of different external forcings and the specific SST change

patterns in the decreasing trend of precipitation, and the related dynamics and thermodynamics.

The current analysis emphasizes the close relationship between vertical motions and the drought conditions in early spring over SE China and presents an observational metric for examining the driving processes. It may serve as a fundamental basis for a better explanation of the variations of drought conditions and for effectively monitoring and forecasting future drought conditions.

**Supplementary Information** The online version contains supplementary material available at <https://doi.org/10.1007/s00382-023-06708-8>.

**Author contributions** The study conception and design were contributed by ZY, SY, and WW. Material preparation and data collection and analysis were performed by ZY and WW. The original draft of manuscript was written by ZY and WW. The review and editing were performed by all authors.

**Funding** This study was supported by the National Key R&D Program of China (2019YFC1510400), the National Natural Science Foundation of China (41975074), the Guangdong Basic and Applied Basic Research Foundation (2023A1515010908, 2020A1515110104), the Guangdong Province Key Laboratory for Climate Change and Natural Disaster Studies (2020B1212060025), and the Innovation Group Project of Southern Marine Science and Engineering Guangdong Laboratory (Zhuhai) (311021001).

**Data availability** The observational datasets are available from the corresponding author on reasonable request. The Medium-range Weather Forecasts fifth major global reanalysis is provided by the European Centre (<https://cds.climate.copernicus.eu/cdsapp#!/dataset/reanalysis-era5-pressure-levels-monthly-means?tab=overview>).

## Declarations

**Conflict of interest** The authors have not disclosed any competing interests.

**Open Access** This article is licensed under a Creative Commons Attribution 4.0 International License, which permits use, sharing, adaptation, distribution and reproduction in any medium or format, as long as you give appropriate credit to the original author(s) and the source, provide a link to the Creative Commons licence, and indicate if changes were made. The images or other third party material in this article are included in the article's Creative Commons licence, unless indicated otherwise in a credit line to the material. If material is not included in the article's Creative Commons licence and your intended use is not permitted by statutory regulation or exceeds the permitted use, you will need to obtain permission directly from the copyright holder. To view a copy of this licence, visit <http://creativecommons.org/licenses/by/4.0/>.

## References

- Abdillah MR, Kanno Y, Iwasaki T (2017) Tropical–extratropical interactions associated with East Asian cold air outbreaks. Part I: interannual variability. *J Clim* 30(8):2989–3007. <https://doi.org/10.1175/jcli-d-16-0152.1>
- Allen RG, Pereira LS, Raes D, Smith M (1998) Crop evapotranspiration: guidelines for computing crop water requirements. FAO Irrigation and Drainage Paper 56. <https://www.fao.org/docrep/X0490E/X0490E00.htm>
- Chen H, Sun J (2015) Changes in drought characteristics over China using the standardized precipitation evapotranspiration index. *J Clim* 28(13):5430–5447. <https://doi.org/10.1175/jcli-d-14-00707.1>
- Chou C, Chiang JCH, Lan C, Chung C, Liao Y, Lee C (2013) Increase in the range between wet and dry season precipitation. *Nat Geosci* 6(4):263–267. <https://doi.org/10.1038/ngeo1744>
- Chung PH, Li T (2013) Interdecadal relationship between the mean state and El Niño. *J Clim* 26(2):361–379. <https://doi.org/10.1175/jcli-d-12-00106.1>
- Cook BI, Smerdon JE, Seager R, Coats S (2014) Global warming and 21st century drying. *Clim Dyn* 43(9–10):2607–2627. <https://doi.org/10.1007/s00382-014-2075-y>
- Dai A, Zhao T (2017) Uncertainties in historical changes and future projections of drought. Part I: estimates of historical drought changes. *Clim Change* 144(3):519–533. <https://doi.org/10.1007/s10584-016-1705-2>
- Dai A, Trenberth KE, Qian TT (2004) A global dataset of palmer drought severity index for 1870–2002: Relationship with soil moisture and effects of surface warming. *J Hydrometeorol* 5(6):1117–1130. <https://doi.org/10.1175/jhm-386.1>
- Deng J, Xu H, Ma H, Jiang Z (2014) Numerical study of the effect of anthropogenic aerosols on spring persistent rain over eastern China. *J Meteorol Res* 28(3):341–353. <https://doi.org/10.1007/s13351-014-3198-0>
- Ding Y, Gong X, Xing Z, Cai H, Zhou Z, Zhang D, Sun P, Shi H (2021) Attribution of meteorological, hydrological and agricultural drought propagation in different climatic regions of China. *Agric Water Manag*. <https://doi.org/10.1016/j.agwat.2021.106996>
- Du J, Wang K, Jiang S, Cui B, Wang J, Zhao C, Li J (2019) Urban dry island effect mitigated urbanization effect on observed warming in China. *J Clim* 32(18):5705–5723. <https://doi.org/10.1175/jcli-d-18-0712.1>
- Du J, Wang K, Cui B (2021) Attribution of the extreme drought-related risk of wildfires in spring 2019 over Southwest China. *Bull Am Meteorol Soc* 102(1):S83–S90. <https://doi.org/10.1175/bams-d-20-0165.1>
- Duan A, Wang M, Lei Y, Cui Y (2013) Trends in summer rainfall over china associated with the Tibetan Plateau sensible heat source during 1980–2008. *J Clim* 26(1):261–275. <https://doi.org/10.1175/jcli-d-11-00669.1>
- Gao H, Yang S (2009) A severe drought event in northern China in winter 2008–2009 and the possible influences of La Niña and Tibetan Plateau. *J Geophys Res*. <https://doi.org/10.1029/2009jd012430>
- Gu L, Chen J, Yin J, Xu C, Chen H (2020) Drought hazard transferability from meteorological to hydrological propagation. *J Hydrol*. <https://doi.org/10.1016/j.jhydrol.2020.124761>
- Hersbach H, Bell B, Berrisford P, Hirahara S, Horanyi A, Munoz-Sabater J, Nicolas J, Peubey C, Radu R, Schepers D, Simmons A, Soci C, Abdalla S, Abellan X, Balsamo G, Bechtold P, Biavati G, Bidlot J, Bonavita M, De Chiara G, Dahlgren P, Dee D, Diamantakis M, Dragani R, Flemming J, Forbes R, Fuentes M, Geer A, Haimberger L, Healy S, Hogan RJ, Holm E, Janiskova M, Keeley S, Laloyaux P, Lopez P, Lupu C, Radnoti G, de Rosnay P, Rozum I, Vamborg F, Villaume S, Thepaut J-N (2020) The ERA5 global reanalysis. *Q J R Meteorol Soc* 146(730):1999–2049. <https://doi.org/10.1002/qj.3803>
- Hu K, Huang G, Wu R, Wang L (2017) Structure and dynamics of a wave train along the wintertime Asian jet and its impact on East Asian climate. *Clim Dyn* 51(11–12):4123–4137. <https://doi.org/10.1007/s00382-017-3674-1>



- Jia X, You Y, Wu R, Yang Y (2019) Interdecadal changes in the dominant modes of the interannual variation of spring precipitation over China in the mid-1980s. *J Geophys Res Atmos* 124(20):10676–10695. <https://doi.org/10.1029/2019jd030901>
- Jia X, Zhang C, Wu R, Qian Q (2020) Influence of Tibetan Plateau autumn snow cover on interannual variations in spring precipitation over southern China. *Clim Dyn* 56(3–4):767–782. <https://doi.org/10.1007/s00382-020-05497-8>
- Jia X, Zhang C, Wu R, Qian Q (2021) Changes in the relationship between spring precipitation in southern China and Tropical Pacific-South Indian ocean SST. *J Clim* 34(15):6267–6279. <https://doi.org/10.1175/jcli-d-20-0817.1>
- Kendall MG (1975) Rank auto-correlation methods. Charles Griffin, London
- Keyantash J, Dracup JA (2002) The quantification of drought: an evaluation of drought indices. *Bull Am Meteorol Soc* 83(8):1167–1180. <https://doi.org/10.1175/1520-0477-83.8.1167>
- Kim J-W, An S, Jun S, Park H, Yeh S (2017) ENSO and East Asian winter monsoon relationship modulation associated with the anomalous northwest Pacific anticyclone. *Clim Dyn* 49(4):1157–1179. <https://doi.org/10.1007/s00382-016-3371-5>
- Li X, Liang W, Wen Z (2010) Characteristics of the atmospheric water vapor and its relationship with rainfall in south China in northern autumn. *J Trop Meteorol* 26(5):626–632
- Li Z, Yang S, He B, Hu C (2016) Intensified springtime deep convection over the South China Sea and the Philippine Sea driest southern China. *Sci Rep*. <https://doi.org/10.1038/srep30470>
- Li P, Zhou T, Chen X (2017) Water vapor transport for spring persistent rains over southeastern China based on five reanalysis datasets. *Clim Dyn* 51(11–12):4243–4257. <https://doi.org/10.1007/s00382-017-3680-3>
- Li L, She D, Zheng H, Lin P, Yang Z-L (2020) Elucidating diverse drought characteristics from two meteorological drought indices (SPI and SPEI) in China. *J Hydrometeorol* 21(7):1513–1530. <https://doi.org/10.1175/jhm-d-19-0290.1>
- Li Y, Zhou W, Yang S, Zhang R, Cheung H, Zhang Y (2022) Recent early-spring drying trend over southern China associated with changes in the zonal thermal contrast over Pacific. *J Clim* 35:1–28. <https://doi.org/10.1175/jcli-d-21-0891.1>
- Liu Y, Feng J, Chen W, Wang L, Xu P (2019) Structural changes in the Pacific-Japan pattern in the late 1990s. *J Clim* 32(2):607–621. <https://doi.org/10.1175/jcli-d-18-0123.1>
- Mann HB (1945) Nonparametric tests against trend. *Econometrica* 13(3):245. <https://doi.org/10.2307/1907187>
- McKee TB, Doesken NJ, Kleist J (1993) The relationship of drought frequency and duration to time scales. American Meteorological Society, Boston, pp 179–183
- Milly PCD, Dunne KA (2016) Potential evapotranspiration and continental drying. *Nat Clim Change*. <https://doi.org/10.1038/nclimate3046>
- Mishra AK, Singh VP (2010) A review of drought concepts. *J Hydrol* 391(1–2):204–216. <https://doi.org/10.1016/j.jhydrol.2010.07.012>
- Montaseri M, Amirataee B (2017) Comprehensive stochastic assessment of meteorological drought indices. *Int J Climatol* 37(2):998–1013. <https://doi.org/10.1002/joc.4755>
- Oh SB, Byun HR, Kim DW (2014) Spatiotemporal characteristics of regional drought occurrence in East Asia. *Theoret Appl Climatol* 117(1–2):89–101. <https://doi.org/10.1007/s00704-013-0980-3>
- Oueslati B, Yiou P, Jezequel A (2019) Revisiting the dynamic and thermodynamic processes driving the record-breaking January 2014 precipitation in the southern UK. *Sci Rep* 9(1):2859. <https://doi.org/10.1038/s41598-019-39306-y>
- Palmer W (1965) Meteorological drought. US Department of Commerce, Weather Bureau, Washington
- Park C, Ho C, Park DR, Park TW, Kim J (2020) Interannual variations of spring drought-prone conditions over three subregions of East Asia and associated large-scale circulations. *Theoret Appl Climatol* 142(3–4):1117–1131. <https://doi.org/10.1007/s00704-020-03371-5>
- Qiang X, Yang X (2013) Relationship between the first rainy season precipitation anomaly in South China and the sea surface temperature anomaly in the Pacific. *Chin J Geophys Chin Edition* 56(8):2583–2593. <https://doi.org/10.6038/cjg20130808>
- Sampe T, Xie S (2010) Large-scale dynamics of the meiyu-baiu rainband: environmental forcing by the westerly jet. *J Clim* 23(1):113–134. <https://doi.org/10.1175/2009jcli3128.1>
- Sen PK (1968) Estimates of the regression coefficient based on Kendall's tau. *J Am Stat Assoc* 63(324):1379–1389. <https://doi.org/10.2307/2285891>
- Song X, Li L, Fu G, Li J, Zhang A, Liu W, Zhang K (2014) Spatial-temporal variations of spring drought based on spring-composite index values for the Songnen Plain Northeast China. *Theoret Appl Climatol* 116(3–4):371–384. <https://doi.org/10.1007/s00704-013-0957-2>
- Spinoni J, Barbosa P, Bucchignani E, Cassano J, Cavazos T, Christensen JH, Christensen OB, Coppola E, Evans J, Geyer B, Giorgi F, Hadjinicolaou P, Jacob D, Katzfey J, Koenigk T, Laprise R, Lennard CJ, Kurnaz ML, Li D, Llopart M, McCormick N, Naumann G, Nikulin G, Ozturk T, Panitz H-J, da Rocha RP, Rockel B, Solman SA, Syktus J, Tangang F, Teichmann C, Vautard R, Vogt JV, Winger K, Zittis G, Dosio A (2020) Future global meteorological drought hot spots: a study based on CORDEX data. *J Clim* 33(9):3635–3661. <https://doi.org/10.1175/jcli-d-19-0084.1>
- Stagge JH, Tallaksen LM, Gudmundsson L, Van Loon AF, Stahl K (2015) Candidate distributions for climatological drought indices (SPI and SPEI). *Int J Climatol* 35(13):4027–4040. <https://doi.org/10.1002/joc.4267>
- Sun C, Yang S (2012) Persistent severe drought in southern China during winter-spring 2011: large-scale circulation patterns and possible impacting factors. *J Geophys Res Atmos*. <https://doi.org/10.1029/2012jd017500>
- Sun S, Chen H, Li J, Wei J, Wang G, Sun G, Hua W, Zhou S, Deng P (2018) Dependence of 3-month standardized precipitation-evapotranspiration index dryness/wetness sensitivity on climatological precipitation over southwest China. *Int J Climatol* 38(12):4568–4578. <https://doi.org/10.1002/joc.5690>
- Suroso ND, Ardiansyah AE (2021) Drought detection in Java Island based on standardized precipitation and evapotranspiration index (SPEI). *J Water Clim Change* 12(6):2734–2752. <https://doi.org/10.2166/wcc.2021.022>
- Tian S, Yasunari T (1998) Climatological aspects and mechanism of spring persistent rains over central China. *J Meteor Soc Jpn* 76:57–71
- Trenberth KE, Dai A, van der Schrier G, Jones PD, Barichivich J, Briffa KR, Sheffield J (2014) Global warming and changes in drought. *Nat Clim Change* 4(1):17–22. <https://doi.org/10.1038/nclimate2067>
- Vicente-Serrano SM (2006) Differences in spatial patterns of drought on different time scales: an analysis of the Iberian Peninsula. *Water Resour Manage* 20(1):37–60. <https://doi.org/10.1007/s11269-006-2974-8>
- Vicente-Serrano SM, Begueria S, Lopez-Moreno JI (2010) A multi-scalar drought index sensitive to global warming: the standardized precipitation evapotranspiration index. *J Clim* 23(7):1696–1718. <https://doi.org/10.1175/2009jcli2909.1>
- Wan R, Zhao B, Wu G (2009) New evidences on the climatic causes of the formation of the spring persistent rains over southeastern China. *Adv Atmos Sci* 26(6):1081–1087. <https://doi.org/10.1007/s00376-009-7202-z>
- Wang B, Wu RG, Fu XH (2000) Pacific-East Asian teleconnection: how does ENSO affect East Asian climate? *J Clim* 13(9):1517–1536.

- [https://doi.org/10.1175/1520-0442\(2000\)013%3c1517:Peathd%3e2.0.Co;2](https://doi.org/10.1175/1520-0442(2000)013%3c1517:Peathd%3e2.0.Co;2)
- Wang B, Luo X, Yang Y, Sun W, Cane MA, Cai W, Yeh S, Liu J (2019) Historical change of El Niño properties sheds light on future changes of extreme El Niño. *Proc Natl Acad Sci U S A* 116(45):22512–22517. <https://doi.org/10.1073/pnas.1911130116>
- Wang S, Zuo H, Sun F, Wu L, Yin Y, Luo J-J (2021) Dynamics of East Asian spring rainband and spring–autumn contrast: environmental forcings of large-scale circulation. *J Clim* 34(9):3523–3541. <https://doi.org/10.1175/jcli-d-20-0501.1>
- Wei W, Zhang R, Wen M, Yang S (2017) Relationship between the Asian westerly jet stream and summer rainfall over central Asia and north China: roles of the Indian monsoon and the South Asian high. *J Clim* 30(2):537–552. <https://doi.org/10.1175/jcli-d-15-0814.1>
- Wen Z, Wu N, Feng Y, Lin L, Yuan Z, Chen B (2007) A quantitative diagnosis for the mechanisms of spring droughts in South China. *Chin J Atmos Sci* 31(6):1223–1236
- Wen D, Yang Y, Cao J (2021) Interdecadal variation of early spring rainfall over the southeastern edge of the Tibetan Plateau. *J Geophys Res Atmos*. <https://doi.org/10.1029/2020jd033058>
- Wu X, Mao J (2016) Interdecadal modulation of ENSO-related spring rainfall over South China by the Pacific Decadal Oscillation. *Clim Dyn* 47(9–10):3203–3220. <https://doi.org/10.1007/s00382-016-3021-y>
- Wu W, Wen Z, Chen Y, Cui S (2012) Interannual variability of winter and spring precipitation in south China and its relation to moisture transport. *J Trop Meteorol* 28(2):187–196
- Xie PP, Yatagai A, Chen MY, Hayasaka T, Fukushima Y, Liu CM, Yang S (2007) A Gauge-based analysis of daily precipitation over East Asia. *J Hydrometeorol* 8(3):607–626. <https://doi.org/10.1175/jhm583.1>
- Xie S, Kosaka Y, Du Y, Hu K, Chowdary JS, Huang G (2016) Indo-western Pacific ocean capacitor and coherent climate anomalies in post-ENSO summer: a review. *Adv Atmos Sci* 33(4):411–432. <https://doi.org/10.1007/s00376-015-5192-6>
- Xin X, Yu R, Zhou T, Wang B (2006) Drought in late spring of South China in recent decades. *J Clim* 19(13):3197–3206. <https://doi.org/10.1175/jcli3794.1>
- Xu K, Yang D, Yang H, Li Z, Qin Y, Shen Y (2015) Spatio-temporal variation of drought in China during 1961–2012: a climatic perspective. *J Hydrol* 526:253–264. <https://doi.org/10.1016/j.jhydrol.2014.09.047>
- Xu B, Li G, Gao C, Yan H, Wang Z, Li Y, Zhu S (2021) Asymmetric effect of El Niño–Southern Oscillation on the spring precipitation over south China. *Atmos*. <https://doi.org/10.3390/atmos12030391>
- You Y, Jia X (2018) Interannual variations and prediction of spring precipitation over China. *J Clim* 31(2):655–670. <https://doi.org/10.1175/jcli-d-17-0233.1>
- Zhang YS, Li T, Wang B (2004) Decadal change of the spring snow depth over the Tibetan Plateau: the associated circulation and influence on the East Asian summer monsoon. *J Clim* 17(14):2780–2793. [https://doi.org/10.1175/1520-0442\(2004\)017%3c2780:Dcotss%3e2.0.Co;2](https://doi.org/10.1175/1520-0442(2004)017%3c2780:Dcotss%3e2.0.Co;2)
- Zhang Q, Yao YB, Wang Y, Wang SP, Wang JS, Yang JH, Wang J, Li YP, Shang JL, Li WJ (2019) Characteristics of drought in Southern China under climatic warming, the risk, and countermeasures for prevention and control. *Theoret Appl Climatol* 136(3–4):1157–1173. <https://doi.org/10.1007/s00704-018-2541-2>
- Zhang L, Chen Z, Zhou T (2021) Human influence on the increasing drought risk over Southeast Asian monsoon region. *Geophys Res Lett*. <https://doi.org/10.1029/2021gl093777>
- Zhang C, Guo Y, Wen Z (2022) Interdecadal change in the effect of Tibetan Plateau snow cover on spring precipitation over Eastern China around the early 1990s. *Clim Dyn* 58(9–10):2807–2824. <https://doi.org/10.1007/s00382-021-06035-w>
- Zhao P, Jiang P, Zhou X, Zhu C (2009) Modeling impacts of East Asian Ocean–Land thermal contrast on spring southwesterly winds and rainfall in eastern China. *Chin Sci Bull* 54(24):4733–4741. <https://doi.org/10.1007/s11434-009-0229-9>
- Zheng J, Liu Q, Wang C, Zheng X (2012) Impact of heating anomalies associated with rainfall variations over the Indo-western Pacific on Asian atmospheric circulation in winter. *Clim Dyn* 40(7–8):2023–2033. <https://doi.org/10.1007/s00382-012-1478-x>
- Zhou H, Zhou W, Liu Y, Yuan Y, Huang J, Liu Y (2020) Identifying spatial extent of meteorological droughts: an examination over a humid region. *J Hydrol*. <https://doi.org/10.1016/j.jhydrol.2020.125505>

**Publisher's Note** Springer Nature remains neutral with regard to jurisdictional claims in published maps and institutional affiliations.